Applied Physics Letters

Ferroelectric-induced resistive switching in ultrathin $(Ba,Sr)TiO_3$ tunnel junctions due to strain modulation

Cite as: Appl. Phys. Lett. **113**, 042905 (2018); https://doi.org/10.1063/1.5024449
Submitted: 01 February 2018 . Accepted: 14 July 2018 . Published Online: 27 July 2018

Hei-Man Yau, Zhongnan Xi, Xinxin Chen, Cheuk Ho Chan, Zheng Wen, and Ji-Yan Dai

Ferroelectric-induced resistive switching in ultrathin $(Ba,Sr)TiO_3$ tunnel junctions due to strain modulation

Hei-Man Yau,[1] Zhongnan Xi,[2] Xinxin Chen,[1] Cheuk Ho Chan,[1] Zheng Wen,[1,2] and Ji-Yan Dai[1,a)]
[1]*Department of Applied Physics, The Hong Kong Polytechnic University, Hung Hom, Kowloon, Hong Kong*
[2]*College of Physics, Qingdao University, Qingdao 266071, China*

(Received 1 February 2018; accepted 14 July 2018; published online 27 July 2018)

Through strain modulation to the $(Ba_{0.8},Sr_{0.2})TiO_3$ (BST) tunnel junction, giant resistive switching was achieved in a Pt/BST/Nb:$SrTiO_3$ (Nb:STO) heterostructure, and the role of ferroelectricity in the resistive switching was studied. When an external compressive strain was added to this heterostructure with a ten-unit-cell-thick BST tunnel layer, the resistive switching mechanism was demonstrated to change from thermionic emission to direct tunneling accompanied by the ferroelectricity enhancement to the BST layer. This reveals the role of strain and ferroelectricity in resistive switching which leads to three orders increase in the ON/OFF current ratio for the BST tunnel layer. These encouraging results not only show the potential to enhance ferroelectricity of BST thin film by strain engineering, but also the crucial role of strain engineering in BST tunnel layer-based memory device applications. *Published by AIP Publishing.* https://doi.org/10.1063/1.5024449

The resistive switching device has recently attracted a great deal of attention due to its potential application in non-volatile memories. In particular, the ferroelectric tunnel junction (FTJ) as resistive memory has been studied owing to its unique electron transport properties, i.e., polarization-induced giant tunneling electroresistance (TER).[1–4] Due to the presence of spontaneous polarization and the ability of field induced switching, FTJs have shown bi-stable resistance states with a good write/read cycle endurance and a long retention of data storage,[5–9] and its memory window (the ratio of the high resistance state to the low resistance state, i.e., the ON/OFF current ratio) exhibits up to 10^4 in magnitude.[8,10–12] Although numerous simulation and experimental results have been reported, there are still insufficient experimental evidence to support the conclusion that the giant resistive switching is solely due to ferroelectric polarization enhancement.[3,13–15] Most reported works about FTJ resistive switching mechanism are based on the correlation between resistance change and ferroelectric switching observed by piezoresponse microscopy.[4,7,16] However, the shortcoming of this observation is the difficulty in distinguishing which of the three elements, namely, migration of oxygen vacancies, ferroelectric switching, and filament formation/rupture, is the main cause of the resistance change.

In metal/ferroelectric/semiconductor (MFS) structure, the giant tunneling electroresistance is critically dependent on the ferroelectric/semiconductor interface.[10,17–19] Unlike resistive random-access memory (ReRAM), the resistance of a tunnel junction is affected by both the potential barrier height and the barrier width. By controlling the depletion region thickness at the surface of the semiconductor electrode via ferroelectric polarization, it is expected that the memory window should be greatly enhanced. In order to directly prove the switching mechanism in MFS-FTJ, there is no doubt that the ferroelectric polarization-induced resistive switching can be verified by tuning the strength of ferroelectricity. Previously, we have investigated the dynamic strain-induced electroresistance in a four-unit-cell-thick $BaTiO_3$ MFS-FTJ by applying mechanical stress to the device. The large memory window (ON/OFF ratio up to 10^7), and particularly the observed strain dependences of tunneling resistance, suggested that $BaTiO_3$ polarization was associated with an efficient modulation of the ON/OFF ratio. This experimental result demonstrated the critical role of ferroelectricity to the resistive switching.

To further study the role of ferroelectricity in ferroelectric-induced resistive switching, it is desirable to select a tunnel layer which can be tuned between paraelectric (or very weak ferroelectric) to ferroelectric by mechanical strain. Barium strontium titanate $(Ba_{1-x},Sr_x)TiO_3$ (BST) is a good choice, since at a certain range of composition, it can be easily tuned between paraelectric and ferroelectric phases by either temperature or strain modulation. On the other hand, BST has wide applications due to its high dielectric constant, low leakage current, long service life, high compatibility with device process, as well as low Curie temperature (T_c).[20–23] Apart from its application to electrically controlled microwave devices, it has also attracted a great deal of interest as being one of the materials in the development of Gigabit era dynamic random access memories (DRAM)[24–26] and resistive switching memory.[25–28] Owing to its low T_c, BST usually acts as an insulating dielectric layer sandwiched by two electrodes, and its resistance states can be obtained in a metal/insulator/metal (MIM) capacitor-like heterostructure similar to ReRAM. Most of the experimental results show that the conductive mechanism of this resistive switching using paraelectric BST is attributed to either the field-enhanced Schottky emission or space-charge limited current flow or Poole–Frenkel (PF) mechanism.

In this work, BST thin films with Sr doping concentration of 20 mol. % are used to study the effect of tetragonality in the TER properties of MFS-type tunnel junction through temperature and strain modulations. By introducing strain to the junction using a specially designed bending device,

a)jiyan.dai@polyu.edu.hk

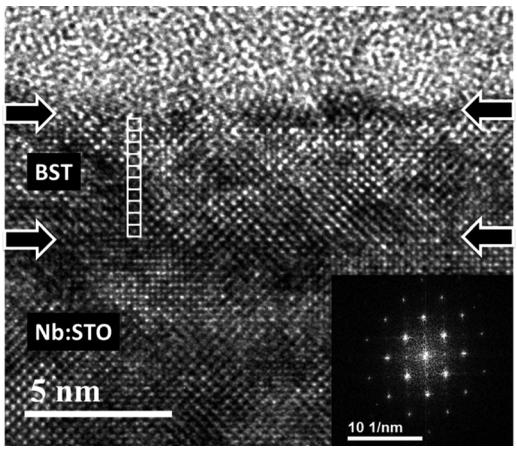

FIG. 1. Structure of BST/Nb:STO heterostructure. High-resolution TEM (HRTEM) image of the ten-unit-cell-thick BST film grown on Nb:STO observed along [100] direction; the inset shows the corresponding FFT pattern.

resistance changes with a very large ON/OFF ratio of the junction are obtained. Our results show that strain modulation offers another approach for BST to be applied in ferroelectric memory devices beyond the present development of DRAM and ReRAM using paraelectric BST.[29]

The $Ba_{0.8}Sr_{0.2}TiO_3$ ultrathin films were epitaxially deposited on a semiconducting (001)-oriented single-crystalline 0.7 wt. % Nb-doped $SrTiO_3$ (Nb:STO) by pulsed-laser deposition using a KrF excimer laser with a wavelength of 248 nm. In order to produce the single-termination step-terrace surface, prior to deposition, the Nb:STO substrates were pre-treated by etching with NH_4F buffered-HF solution and then annealed at 1223 K for an hour in flowing O_2. With the existence of single-termination step-terrace surface, the films were grown with a 2.5 J cm^{-2} laser energy density at 2 Hz repetition, and the substrate temperature was kept at 1043 K with O_2 pressure of 5×10^{-3} mbar. To form MFS structured junctions, metallic top electrodes Pt with 30 μm diameter were deposited on the film's surface by magnetron sputtering at room temperature with a shadow mask.

Figure 1 shows a high-resolution cross-sectional transmission electron microscopy (TEM) image of the BST film on the Nb:STO substrate. One can see that the BST film is epitaxially grown on the substrate, and a continuous layer of about 4-nm-thick (corresponding to ten unit-cells) BST, on top of Nb:STO, can be identified. The inset is the FFT pattern corresponding to the Nb:STO and BST lattices, where one can see that there is basically no split of diffraction spots. This is an indication that the finite amount of Ba doping into the STO lattice, forming the BST film, results in little change of lattice spacing, and the BST film without bending has no or very little ferroelectric polarization.

It is known that the Curie temperature of the BST drops from $T_{cBTO} \sim 400$ K to $T_{cSTO} \sim 0$ K by increasing the proportion of Sr. Due to its low Curie temperature, BST has been used as an insulating paraelectric layer in memory application at room temperature. To demonstrate the strain induced enhancement of ferroelectricity of the ultrathin BST film, the piezoresponse force microscopy (PFM) measurement was carried out at room temperature to observe polarization switching and domain structure of BST. Figure 2 shows the PFM results of the BST film before and after bending. One can see from Figs. 2(a) and 2(b) that, before applying an external stress, only very weak PFM signal can be detected, suggesting that the BST has no sign of ferroelectricity but rather extrinsic contributions due to charge injection (with characteristic diffuse boundaries and enhanced amplitude after writing). By contrast as shown in Figs. 2(d)–2(f), an *in-situ* bending of the sample results in a very strong piezoelectric response. The topography in Fig. 2(c) shows the flat surface of the ultrathin BST/Nb:STO heterostructure with a root-mean-square roughness of 0.11 nm, and the out-of-plane amplitude and phase hysteresis loops can be observed clearly as shown in Fig. 2(d). From this result, coercive voltages of +2.97 V and −1.38 V can be obtained at the minimum of the amplitude signal. Ferroelectric domain structure written on BST with ±5 V exhibits a 180° phase contrast and the amplitude minimum at the domain wall, revealing an antiparallel domain structure. These results confirm the enhancement of ferroelectricity after bending.

In order to study the effect of external stress/strain to the ferroelectric properties of the BST film, a long bar sample with a dimension of 0.5-mm-thick and 10 (length) × 2.5

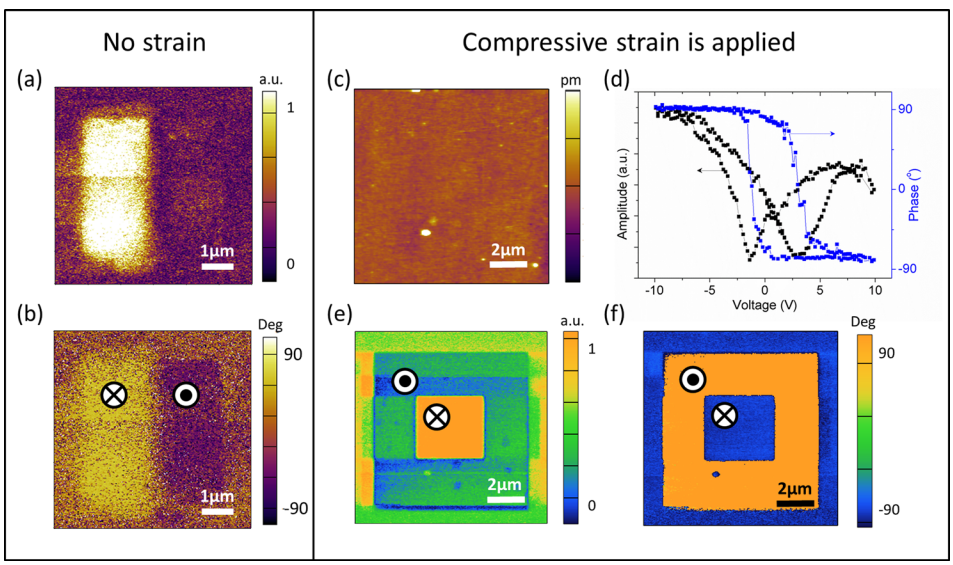

FIG. 2. Topography and ferroelectric properties of the BST film deposited on the Nb:STO substrate before and after bending. (a) PFM out-of-plane amplitude and (b) phase images of the ten-unit-cell-thick BST film on NSTO substrate before any strain is applied. (c) Morphology of the BST surface; (d) PFM amplitude and phase hysteresis loops; (e) PFM out-of-plane amplitude, and (f) phase images recorded after writing an area of 8×8 μm^2 outer square with −5 V and 4×4 μm^2 inner region with +5 V using a biased conductive tip at room temperature.

(width) mm^2 was cut. The reason for using a long bar is because we hold the assumption that by having a longer bar sample, shear stress and strain can be neglected.[30] The sample was bent into u-shaped by a designed tool as schematically illustrated in Fig. 3(a), through which the tetragonality of the BST ultrathin film is expected to be increased by increasing the force along the z direction. The in-plane strain is deducted by $\varepsilon = \Delta L/L = (a_{stressed} - a_0)/a_0$, which is the strain calculated from the distance change ΔL in the bending curvature of the BST layer observed using an optical surface profiler.[31]

With the bottom electrode grounded throughout the measurement, a positive voltage was added from the top electrode to set the junction to low resistance state (ON state). To reset the junction to a high resistance state (OFF state), a negative voltage was applied to the top electrode. Figure 3 shows that, at room temperature, the ratio of electroresistance change increases when strain modulation is applied, and the corresponding ON/OFF ratio as a function of strain is plotted in Fig. 3(b). It is apparent that, by adding compressive strain to the sample, the ON/OFF ratio increases by nearly three orders. The current-voltage (I-V) curves of the ON and OFF states of the Pt/BST/Nb:STO junction under various strains are shown in Figs. 3(c) and 3(d), respectively. The OFF-state currents in Fig. 3(d) show a clear rectifying characteristic. This is in agreement with Wen's report that the junction current is suppressed by the Schottky barrier induced at the ferroelectric/semiconductor interface when ferroelectric polarization is pointing away from the Nb:STO.[17]

It can be noted that the I-V characteristics of the non-strained curve in the ON state [Fig. 3(c)] show a similar asymmetric and rectifying behavior which is similar to the graph plotted for the OFF state. This suggests that the Schottky barrier is prominent and no ferroelectric tunneling is observed in Pt/BST/Nb:STO heterostructure without external strain added. This evidence is in line with the linear relationship of current transportation in the plot of ln(J) vs $\sqrt{E}$ for both ON-and OFF-states non-strained I-V curves when thermionic emission (TE) is dominant in the experiment,[32] i.e., the resistive switching is originated from thermionic emission instead of tunneling. This can be understood by considering the fact that there is no ferroelectricity signal detected initially [as shown in Figs. 2(a) and 2(b)], and positive bound charges induced in the BST/Nb:STO interface are not sufficient enough to drive the n-type semiconductor surface into accumulation. On the other hand, when strain is applied, the ON-state I-V curves are relatively symmetric for the forward and reverse bias. This is due to the fact that being more compressively strained, the ferroelectric polarization is strengthened, and therefore, the n-type semiconductor surface is driven into accumulation resulting in a low resistance state.

Strain-dependent current characteristics at a low voltage under different strains are fitted into the direct tunneling model, i.e., Brinkman's model[33] and Gruverman's model.[7] In these fitting models, direct tunneling through the barrier with interfacial effects is assumed to depend on the ferroelectric polarization direction

$$I_{DT} = \mathrm{SC}\frac{\exp\left\{\alpha\left[\left(\varphi_2 - \frac{eV}{2}\right)^{\frac{3}{2}} - \left(\varphi_1 + \frac{eV}{2}\right)^{\frac{3}{2}}\right]\right\}}{\alpha^2\left[\left(\varphi_2 - \frac{eV}{2}\right)^{\frac{1}{2}} - \left(\varphi_1 + \frac{eV}{2}\right)^{\frac{1}{2}}\right]} \times \sinh\left\{\frac{3eV}{4}\alpha\left[\left(\varphi_2 - \frac{eV}{2}\right)^{\frac{1}{2}} - \left(\varphi_1 + \frac{eV}{2}\right)^{\frac{1}{2}}\right]\right\}, \quad (1)$$

$$\text{with} \quad \mathrm{C} = -\frac{32\pi e m^*}{9h^3}, \quad (2)$$

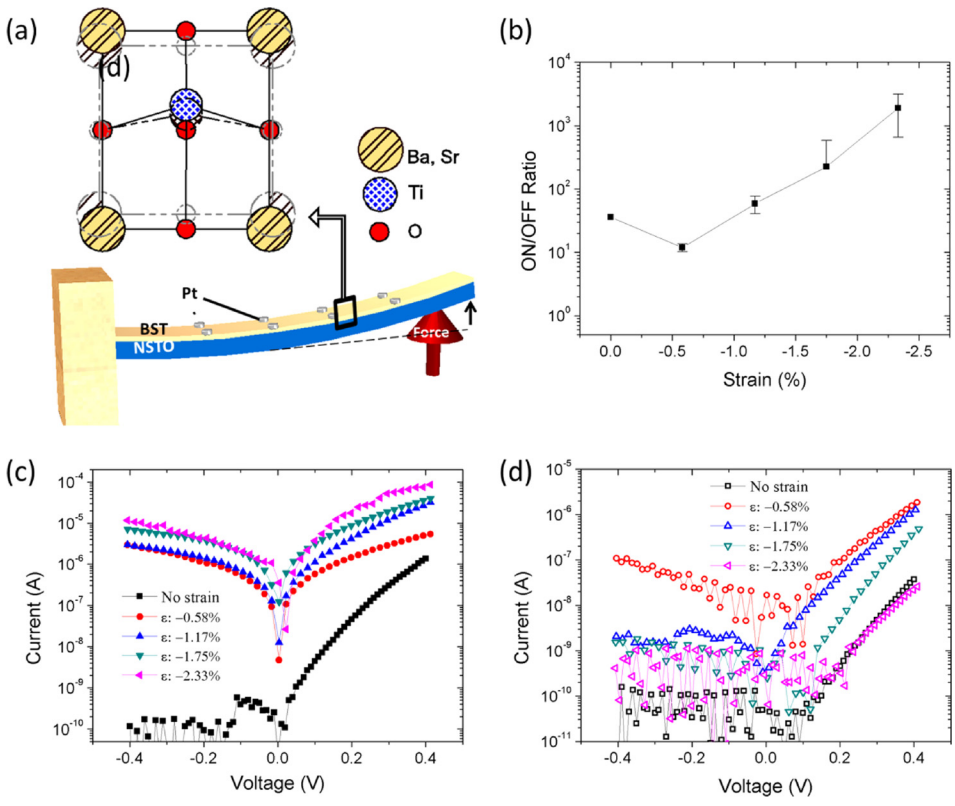

FIG. 3. TER and current-voltage characteristic at room temperature. (a) Schematic description of the experimental setup for strain engineering induced by the external bending force; (b) ON/OFF ratios as a function of strain; I-V curve with different strain modulations of the (c) ON and (d) OFF states.

$$\text{and} \quad \alpha = \frac{8\pi d(2m^*)^{\frac{1}{2}}}{3h(\varphi_1 + eV - \varphi_2)}, \tag{3}$$

where I_{DT} is the direct tunneling current given by Gruverman *et al.*, S the area of the interface, d the film thickness, h the Planck constant, m^* the effective carrier mass, and φ_1 and φ_2 the potential barrier heights at the interface.

When an external force is added to the sample along the z direction, the in-plane compressive strain on the BST film results in an increased tetragonality (c/a ratio) and induces ferroelectric polarization, as shown in Figs. 2(d)–2(f). Consequently, the ferroelectric polarization pointing to Nb:STO induces positive charges at the BST/Nb:STO interface and drives the Nb:STO surface into accumulation. In this situation, the Nb:STO surface can be treated as a metal contact which results in a reduced potential barrier across the ultrathin tunnel layer, and therefore, the tunneling probability increases and the junction is in the ON state.[4]

As shown in Fig. 4(a), with polarization-induced interfacial effects, the fitting result agrees well with the mechanism of direct tunneling through the barrier. The mean potential barrier height was calculated, and the results point to the conclusion that when compressive strain increases, the barrier height decreases [Fig. 4(b)]. The decreased barrier height suggests enhanced ferroelectric polarization in BST pointing towards the bottom electrode, and the enhanced ferroelectricity is attributed to the additional in-plane compressive strain leading to a higher degree of tetragonality of BST.

On the contrary, when the polarization is reversed towards the top electrode, a depletion layer acting as an extra barrier will be formed at the BST/Nb:STO interface. By fitting the forward biased current characteristic with thermionic emission (TE) model, the barrier height and width of the depletion layer are determined as shown in Fig. 4(c). The forward biased currents are described by the TE theory as follows:

$$I_{forward} = SA^*T^2\exp\left(-\frac{\varepsilon\varphi_B}{kT}\right)\left[\exp\left(\frac{qV}{nk_BT}\right) - 1\right], \tag{4}$$

where S is the junction area, A^* the Richardson constant, T the absolute temperature, q the electron charge, k the Boltzmann constant, n the ideal factor, and φ_B the Schottky barrier height. From the linear relationship in TE modeling, we can identify the barrier height in the OFF state using Eq. (4). The corresponding depletion region width can be estimated using the following equation:

$$W_D = \left[\frac{2\varepsilon_s}{qN_D}(V_{bi} - V)\right]^{\frac{1}{2}}, \tag{5}$$

where W_D is the depletion region width, ε_s the dielectric constant of $Nb:SrTiO_3$, N_D the donor concentration,[34] $V_{bi} = \varphi_B + \varphi_n$, and $\varphi_n = E_F - E_c = 0.19\,\text{eV}$, as previously reported.[35] Negative bound charges in the ferroelectric tunnel barrier results in an increased depletion width of the Nb:STO surface, and in the meantime, incomplete screening at the Nb:STO interface increases the barrier height. As a result, tunneling current decreased significantly, and the tunnel junction becomes a high resistance OFF state.

In the OFF state, the development of ferroelectric-induced charges at the interface is attributed to be cause of the barrier width increase. When the sample is bent further and the BST film becomes more compressively stained, stronger polarization towards the top electrode results in increases in barrier height; while at the interface of BST/Nb:STO, the depletion layer widens as more negative bound charges are induced. Figure 4(d) indicates the relationship of the barrier height and the corresponding width of the depletion region as a function of strain, where one can see that both figures increase when strain becomes more compressive. By combining these two states, one can deduce that the ON/OFF ratio increases due to the compressive strain-induced increase in BST's ferroelectricity.

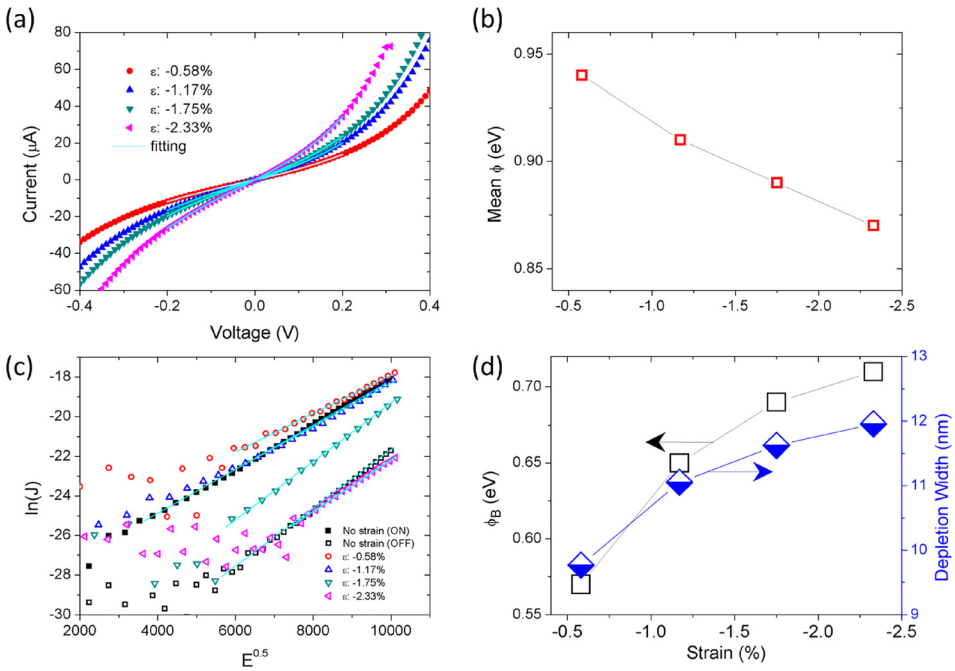

FIG. 4. *I-V* curves fitting of Pt/BST/Nb:STO FTJs with various strain. *I-V* curve fitted by (a) the direct tunneling model[7,33] and (c) the thermionic emission model;[32] (b) the corresponding calculated mean barrier height in the ON state and (d) calculated potential barrier height and width of the depletion region in the OFF state.

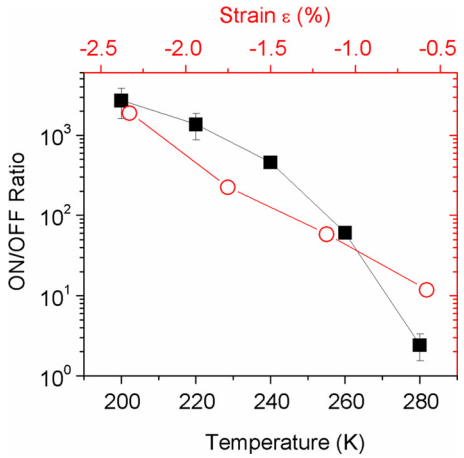

FIG. 5. Temperature- and strain-dependent ON/OFF ratios of the Pt/BST/Nb:STO tunnel junction.

To further investigate the ferroelectricity induced polarization in BST-FTJ, resistive switching was tested at reduced temperatures ranging from 220 to 280 K, and the corresponding temperature-dependent ON/OFF ratio is shown in Fig. 5. The result suggests that the structure of BST changes to a higher degree of tetragonality during cooling and the ferroelectric polarization of the BST layer is enhanced at a lower temperature. In the ON state, the enhanced ferroelectric polarization results in reduced barrier height, while in the OFF state, the barrier becomes wider due to enhanced polarization at lower temperatures. By combining these two states, the ON/OFF ratio of the junction is increased up to 10^3 due to cooling.

In conclusion, strain-dependent ferroelectric tunneling in BST-based FTJs has been studied. It is revealed that the ON/OFF ratio of the FTJ's tunneling resistance can be increased up to three orders of magnitudes by adding compressive strain through mechanical bending. It also revealed that the compressive strain greatly enhanced the ferroelectricity of the BST tunnel layer whose pristine state is paraelectric or very weak ferroelectric. These results prove the role of ferroelectricity in the BST tunnel junction and suggest a mechanical approach to modulate the tunneling characteristics of FTJs.

This work was supported by the RGC (Grant No. NSFC/RGC 517/14), The Hong Kong Polytechnic University Strategic Importance Project (No. 1-ZE25), and the Internal Grant No. 1-BBAF. Z.W. acknowledges financial support from the Natural Science Foundation of Shandong (Grant No. ZR2017JL001) and an Innovation Project of Qingdao (No. 17-1-1-71-jch). We thank K. O. Cheung and C. M. Wong for useful comments on the manuscript.

[1]E. Y. Tsymbal and H. Kohlstedt, Science **313**, 181 (2006).
[2]E. Y. Tsymbal, A. Gruverman, V. Garcia, M. Bibes, and A. Barthélémy, MRS Bull. **37**, 138 (2012).
[3]D. Pantel and M. Alexe, Phys. Rev. B **82**, 134105 (2010).
[4]M. Zhuravlev, R. Sabirianov, S. Jaswal, and E. Tsymbal, Phys. Rev. Lett. **94**, 246802 (2005).
[5]L. Jiang, W. S. Choi, H. Jeen, S. Dong, Y. Kim, M. G. Han, Y. Zhu, S. V. Kalinin, E. Dagotto, T. Egami, and H. N. Lee, Nano Lett. **13**, 5837 (2013).
[6]W. Jin Hu, Z. Wang, W. Yu, and T. Wu, Nat. Commun. **7**, 10808 (2016).
[7]A. Gruverman, D. Wu, H. Lu, Y. Wang, H. W. Jang, C. M. Folkman, M. Y. Zhuravlev, D. Felker, M. Rzchowski, C. B. Eom, and E. Y. Tsymbal, Nano Lett. **9**, 3539 (2009).
[8]D. J. Kim, H. Lu, S. Ryu, C.-W. Bark, C.-B. Eom, E. Y. Tsymbal, and A. Gruverman, Nano Lett. **12**, 5697 (2012).
[9]A. Chanthbouala, V. Garcia, R. O. Cherifi, K. Bouzehouane, S. Fusil, X. Moya, S. Xavier, H. Yamada, C. Deranlot, N. D. Mathur, M. Bibes, A. Barthélémy, and J. Grollier, Nat. Mater. **11**, 860 (2012).
[10]Z. Wen, C. Li, D. Wu, A. Li, and N. Ming, Nat. Mater. **12**, 617 (2013).
[11]Z. Wen, D. Wu, and A. Li, Appl. Phys. Lett. **105**, 052910 (2014).
[12]S. Boyn, A. M. Douglas, C. Blouzon, P. Turner, A. Barthélémy, M. Bibes, S. Fusil, J. M. Gregg, and V. Garcia, Appl. Phys. Lett. **109**, 232902 (2016).
[13]C.-L. Jia, V. Nagarajan, J.-Q. He, L. Houben, T. Zhao, R. Ramesh, K. Urban, and R. Waser, Nat. Mater. **6**, 64 (2007).
[14]L. Li, J. Britson, J. R. Jokisaari, Y. Zhang, C. Adamo, A. Melville, D. G. Schlom, L. Q. Chen, and X. Pan, Adv. Mater. **28**, 6574 (2016).
[15]V. Garcia and M. Bibes, Nat. Commun. **5**, 4289 (2014).
[16]A. Chanthbouala, A. Crassous, V. Garcia, K. Bouzehouane, S. Fusil, X. Moya, J. Allibe, B. Dlubak, J. Grollier, S. Xavier, C. Deranlot, A. Moshar, R. Proksch, N. D. Mathur, M. Bibes, and A. Barthélémy, Nat. Nanotechnol. **7**, 101 (2012).
[17]Z. Xi, J. Ruan, C. Li, C. Zheng, Z. Wen, J. Dai, A. Li, and D. Wu, Nat. Commun. **8**, 15217 (2017).
[18]C. Li, L. Huang, T. Li, W. Lü, X. Qiu, Z. Huang, Z. Liu, S. Zeng, R. Guo, Y. Zhao, K. Zeng, M. Coey, J. Chen, Ariando, and T. Venkatesan, Nano Lett. **15**, 2568 (2015).
[19]X. Liu, J. D. Burton, and E. Y. Tsymbal, Phys. Rev. Lett. **116**, 197602 (2016).
[20]A. Kozyrev, A. Ivanov, T. Samoilova, O. Soldatenkov, K. Astafiev, and L. C. Sengupta, J. Appl. Phys. **88**, 5334 (2000).
[21]W. Chang, S. W. Kirchoefer, J. M. Pond, J. S. Horwitz, and L. Sengupta, J. Appl. Phys. **92**, 1528 (2002).
[22]A. Ioachim, M. I. Toacsan, L. Nedelcu, M. G. Banciu, C. A. Dutu, M. Buda, F. Sava, M. Popescu, N. Scarisoreanu, and M. Dinescu, Rom. J. Inf. Sci. Technol. **10**, 347 (2007).
[23]K. Nadaud, C. Borderon, R. Gillard, E. Fourn, R. Renoud, and H. W. Gundel, Thin Solid Films **591**, 90 (2015).
[24]T. Kuroiwa, Y. Tsunemine, T. Horikawa, T. Makita, J. Tanimura, N. Mikami, and K. Sato, Jpn. J. Appl. Phys. **33**, 5187 (1994).
[25]S. Ezhilvalavan and T. Y. Tseng, Mater. Chem. Phys. **65**, 227 (2000).
[26]C. S. Hwang, S. O. Park, H. J. Cho, C. S. Kang, H. K. Kang, S. I. Lee, and M. Y. Lee, Appl. Phys. Lett. **67**, 2819 (1995).
[27]D. S. Jeong, R. Thomas, R. S. Katiyar, J. F. Scott, H. Kohlstedt, A. Petraru, and C. S. Hwang, Rep. Prog. Phys. **75**, 076502 (2012).
[28]G. W. Dietz, M. Schumacher, R. Waser, S. K. Streiffer, C. Basceri, and A. I. Kingon, J. Appl. Phys. **82**, 2359 (1997).
[29]W. Shen, R. Dittmann, and R. Waser, J. Appl. Phys. **107**, 094506 (2010).
[30]W. Ma and L. E. Cross, Appl. Phys. Lett. **82**, 3293 (2003).
[31]H. M. Yau, Z. Xi, X. Chen, Z. Wen, G. Wu, and J. Y. Dai, Phys. Rev. B **95**, 214304 (2017).
[32]P. R. Emtage and W. Tantraporn, Phys. Rev. Lett. **8**, 267 (1962).
[33]W. F. Brinkman, J. Appl. Phys. **41**, 1915 (1970).
[34]K. G. Rana, V. Khikhlovskyi, and T. Banerjee, Appl. Phys. Lett. **100**, 213502 (2012).
[35]Z. Sroubek, Phys. Rev. B **2**, 3170 (1970).